Journal of the Physical Society of Japan **88**, 074704 (2019)
https://doi.org/10.7566/JPSJ.88.074704

Study of the Pressure-Induced Second Superconducting Phase of $(NH_3)_yCs_{0.4}FeSe$ with Double-Dome Superconductivity

Yoshiya Yamamoto[1], Hitoshi Yamaoka[2], Seiichiro Onari[3], Masahiro Yoshida[1], Naohisa Hirao[4], Saori Kawaguchi[4], Yasuo Oishi[4], Xiao Miao[3], Yoshihiro Kubozono[3], Jung-Fu Lin[5,6], Nozomu Hiraoka[7], Hirofumi Ishii[7], Yen-Fa Liao[7], Ku-Ding Tsuei[7], and Jun'ichiro Mizuki[1]

[1]*Graduate School of Science and Technology, Kwansei Gakuin University, Sanda, Hyogo 669-1337, Japan*
[2]*RIKEN SPring-8 Center, Sayo, Hyogo 679-5148, Japan*
[3]*Research Institute for Interdisciplinary Science, Okayama University, Okayama 700-8530, Japan*
[4]*Japan Synchrotron Radiation Research Institute, Sayo, Hyogo 679-5198, Japan*
[5]*Department of Geological Sciences, The University of Texas at Austin, Austin, TX 78712, U.S.A.*
[6]*Center for High Pressure Science and Technology Advanced Research (HPSTAR), Shanghai 201203, China*
[7]*National Synchrotron Radiation Research Center, Hsinchu 30076, Taiwan*

(Received January 24, 2018; revised December 17, 2018; accepted May 21, 2019; published online June 19, 2019)

The pressure dependence of the crystal and electronic structures of $(NH_3)_yCs_{0.4}FeSe$, which has two pressure-induced superconducting domes of the SC1 and SC2 phases, was investigated by x-ray diffraction and emission spectroscopy at low temperatures. We found a pressure-induced change in the crystal structure from tetragonal (T) to collapsed tetragonal (cT) and peculiar pressure dependence of the magnetic moment between the SC1 and SC2 phases at a low temperature. The electronic structure also markedly changed between the two phases. The results suggest that the increase in the electron–electron correlation accompanying the increase in the magnetic moment may relate the high T_c in the SC2 phase. Theoretical calculations using the multi-orbital Hubbard model revealed that the spin susceptibility decreases in the SC1 phase and increases in the SC2 phase with the T → cT phase transition.

1. Introduction

Both hydrostatic and chemical pressure play an important role in tuning the superconducting and magnetic properties of the iron-based superconductors through the lattice degrees of freedom. Iron-based superconductors show complexity in their magnetism and its relationship with superconductivity because all five Fe 3*d* orbitals in the compounds participate in forming the Fermi surface, in contrast to cuprate superconductors, where a single Cu $d_{x^2-y^2}$ orbital mainly dominates superconducting properties.[1)] In striking contrast to other iron-based superconductors, the FeSe system is structurally simple and exhibits nematic ordering without magnetic ordering in the parent phase, whose relationship with its superconductivity remains unclear.[2,3)]

In metal-intercalated FeSe, pressure induces an interesting change in the superconducting transition temperature (T_c). In $A_xFe_{2-y}Se_2$ (A = alkaline metal and Tl) and $(NH_3)_yM_xFeSe$ (M = alkaline metal), T_c decreases with increasing pressure and superconductivity disappears around 10–12 GPa. However, upon further increasing the pressure, a second superconducting phase (SC2) suddenly emerges.[4,5)] Moreover, the maximum T_c for the SC2 phase is higher than that for the lower-pressure phase (SC1). This behavior is reminiscent of MFe_2As_2 (M = Eu, alkaline earth metal) systems, where the tetragonal (T) to collapsed tetragonal (cT) phase transition commonly occurs at room temperature[6)] and the SC2 phase emerges above 13 GPa, where the switch of the carrier type from hole- to electron-like as a result of Fermi surface reconstruction is associated with the T → cT phase transition.[7,8)] The $K_xFe_{2-y}Se_2$ system also shows the possibility of the T → cT phase transition at room temperature.[9)] On the other hand, in $(NH_3)_yM_xFeSe$, the T → cT transition has not been observed at room temperature.[5)] Thus, the physical properties of $(NH_3)_yM_xFeSe$ appear to be different from those of the other double-dome iron-based superconductors, and the origin of the SC2 phase of $(NH_3)_yM_xFeSe$ still remains as an unsolved puzzle. To obtain a universal understanding of the origin of the SC2 phase, which may reveal the mysterious superconducting mechanism in iron-based compounds, it should be clarified whether or not the lattice structure in the SC2 superconducting phase is cT and how the spin state of the Fe-3*d* orbital evolves under pressure in the superconducting phase, particularly the SC2 phase. To address these questions, experiments to directly observe the lattice, electronic structures, and spin state under pressure at low temperatures where the superconductivity actually occurs are necessary.

Here, we performed x-ray diffraction (XRD) and high-resolution x-ray spectroscopy measurements on $(NH_3)_yM_x$-FeSe under pressure at low temperatures. X-ray emission and absorption spectroscopy (XES and XAS) allowed us to study the electronic structure of 3*d* electrons such as the spin state and orbital nature. Although no pressure-induced structural transition has been observed at room temperature,[5)] we found a T → cT phase transition at a low temperature. A pressure-induced change in the electronic structure, which could originate from the T → cT phase transition, was also observed and the physical properties of $(NH_3)_yCs_{0.4}FeSe$ were very different from FeSe.[10)] Theoretical calculations using the multi-orbital Hubbard model succeeded in explaining these experimental results qualitatively.

2. Experiment

$(NH_3)_yCs_{0.4}FeSe$ samples were prepared using a liquid ammonia method.[5,11,12)] The samples were carefully treated in an Ar-filled glove box because of their chemical instability in air. The pressure dependence of the XRD pattern was measured at the SPring-8 BL10XU beamline using a diamond anvil cell with an imaging plate detector in the pressure range of 0–38 GPa at 8 K. XES and XAS measurements in the partial fluorescence mode (PFY-XAS) were

performed under pressure at low temperatures at SPring-8 BL12XU.[9,13] Details of the experiments are described in the supplementary information.[10]

In the theoretical calculation, we employed the ten-orbital (ten Fe d orbitals) tight-binding model for each pressure based on first-principles calculation. The first-principles calculations were performed for the $Cs_{0.5}FeSe$ system for simplicity. Using the random phase approximation (RPA), the spin susceptibility $\hat{\chi}^s(q) = \hat{\chi}^0(q)/[1 - \hat{\Gamma}^s\hat{\chi}^0(q)]$ for the itinerant electrons was calculated using the multi-orbital Hubbard model,[14,15] where $\hat{\Gamma}^s$ is the bare Coulomb interaction for the spin and $\hat{\chi}^0(q)$ is the irreducible susceptibility without self-energy correction. The constraint condition $U = U' + 2J$ was used, where U (U') is the intra- (inter-) orbital interaction and J is the exchange interaction. Hereafter, we fix the values $U = 1.06$ eV and $J/U = 0.12$ in agreement with the first-principles calculations.[16] The spin Stoner factor α^s, which is the maximum eigenvalue of $\hat{\Gamma}^s\hat{\chi}^0(q)$, was also calculated as a function of pressure.

3. Results and Discussion

Figure 1(a) shows the pressure dependence of the XRD pattern at 8 K. A few undesirable peaks (marked with arrows) from the rhenium gasket appear above 16.6 GPa, while other peaks shift smoothly and no additional peaks appear with increasing pressure. Therefore, the crystal structure with the $I4/mmm$ symmetry does not change with pressure in the pressure range of 0–38 GPa. Previous measurements at room temperature also showed no pressure-induced structural change.[5] Rietveld analysis of the spectrum at 0.74 GPa showed that β-FeSe and α-FeSe were included in the sample with mole ratios of 39 and 9%, respectively.[10,17] The lowest angle peak (<1 Å^{-1}) is assigned as the (002) reflection of $(NH_3)_yCs_{0.4}FeSe$ phase which is well separated from the other peaks. This (002) peak intensity decreases with pressure, but it is left clearly in the SC2. Namely, the superconducting phase, $(NH_3)_yCs_{0.4}FeSe$, remains even in the SC2 phase. Figure 1(c) shows change in the lattice parameters calculated using the (002), (114), (116), and (316) reflections, which have minor contributions from the β-FeSe and α-FeSe phases.[10] Note that the Rietveld analysis of the high-pressure data is difficult owing to peak broadening. The lattice constants along the a- and c-axes decrease with pressure as shown in Fig. 1(c). The trend for the lattice constant along the c-axis seems to change above 12 GPa. The pressure dependence of the lattice constants and the volume are well fitted with the Birch–Murnaghan equation at the whole pressure range (see Supplement). On the other hand, plot of c/a against pressure clearly indicates the pressure-induced structural change around 12 GPa at 8 K, as shown in Fig. 1(d). Therefore, the phase diagram with pressure can be divided into the SC1 and SC2 phases. Moreover, it was found that the lattice constant of $c = 14$ Å may be a critical value to divide the superconducting phase into SC1 and SC2.[18] Our result also shows the pressure-induced structural change (T → cT) at $c = 14$ Å where the pressure is approximately 12 GPa. The presence of structural transition observed in the present experiment may be related to this phenomenological $c = 14$ Å rule. The c-axis in SC1 phase easily contracts, in contrast to that in SC2. Thus, we conclude that a T → cT phase transition occurs around 12 GPa at low temperatures.

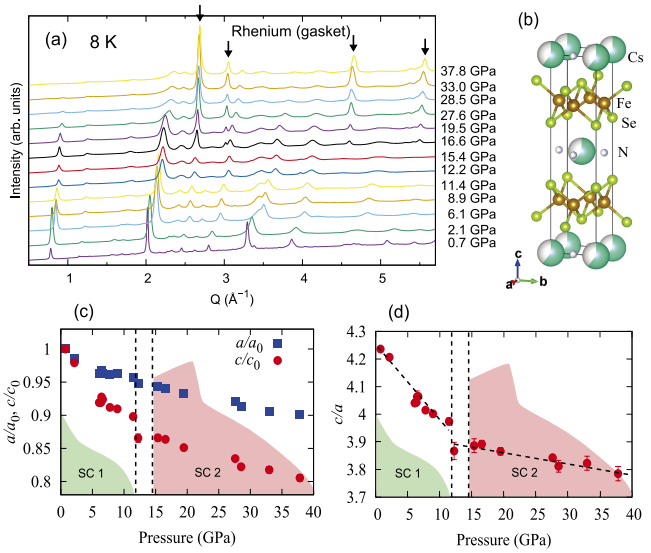

Fig. 1. (Color online) (a) Pressure dependence of the XRD pattern at 8 K. Above 16.6 GPa, a few undesirable peaks (marked with arrows) from the rhenium gasket are observed. (b) Crystal structure of $(NH_3)_yCs_{0.4}FeSe$. (c) Pressure dependence of the lattice constants a/a_0 and c/c_0. The magnitude of the error is the same as the size of the marks. (d) Pressure dependence of the ratio c/a. Dashed lines are guide for eye. Pale green and red regions indicate the two superconductivity domes of the SC1 and SC2 phases, respectively.[5]

This suggests that the shrinkage along the c-axis may occur easily at SC1, corresponding to the rapid decrease in T_c in SC1. Although the superconducting volume fraction in the SC2 is not clear, we observed the T → cT transition at 12 GPa by taking the Bragg peak of $(NH_3)_yCs_{0.4}FeSe$ into account selectively from the FeSe phase.

Figure 2(a) shows the pressure dependence of the Fe $K\beta$ emission spectrum at 20 K. The Fe $K\beta$ spectrum consists of the main peak of $K\beta_{1,3}$ and a broad satellite component of $K\beta'$. The intensity of the $K\beta_{1,3}$ peak increases and that of the $K\beta'$ peak decreases with increasing pressure. This indicates that the Fe local magnetic moment decreases with increasing pressure.[19] We estimated the integrated absolute difference (IAD) to investigate the change in the spin states and local Fe magnetic moment.[19] It is known that the IAD value is proportional to the local magnetic moment in iron-based superconductors with tetrahedral coordination.[20] Figure 2(b) shows the differences between the spectra of $(NH_3)_yCs_{0.4}$-FeSe and FeCrAs, where FeCrAs was used as a reference with a local magnetic moment of $0\mu_B$. The IAD decreases rapidly with increasing pressure in SC1 as shown in Fig. 2(d). However, the IAD increases slowly with pressure in SC2 and then decreases above 24 GPa. Since these $K\beta$ spectra are composed by $(NH_3)_yCs_{0.4}FeSe$ and impurity FeSe phases, we cannot directly discuss the superconducting phase. However, it is known that in FeSe the IAD values decreased monotonically with pressure,[21,22] and thus this anomalous behavior may be caused by the superconducting phase of $(NH_3)_yCs_{0.4}FeSe$.[10] The observed result that the behavior of the magnetic moment under pressure is different for SC1 and SC2 suggests that the spin states of SC1 and SC2 are different as a consequence of the difference in the electronic states. The local magnetic moment generally originates through the Coulomb interaction of electrons and

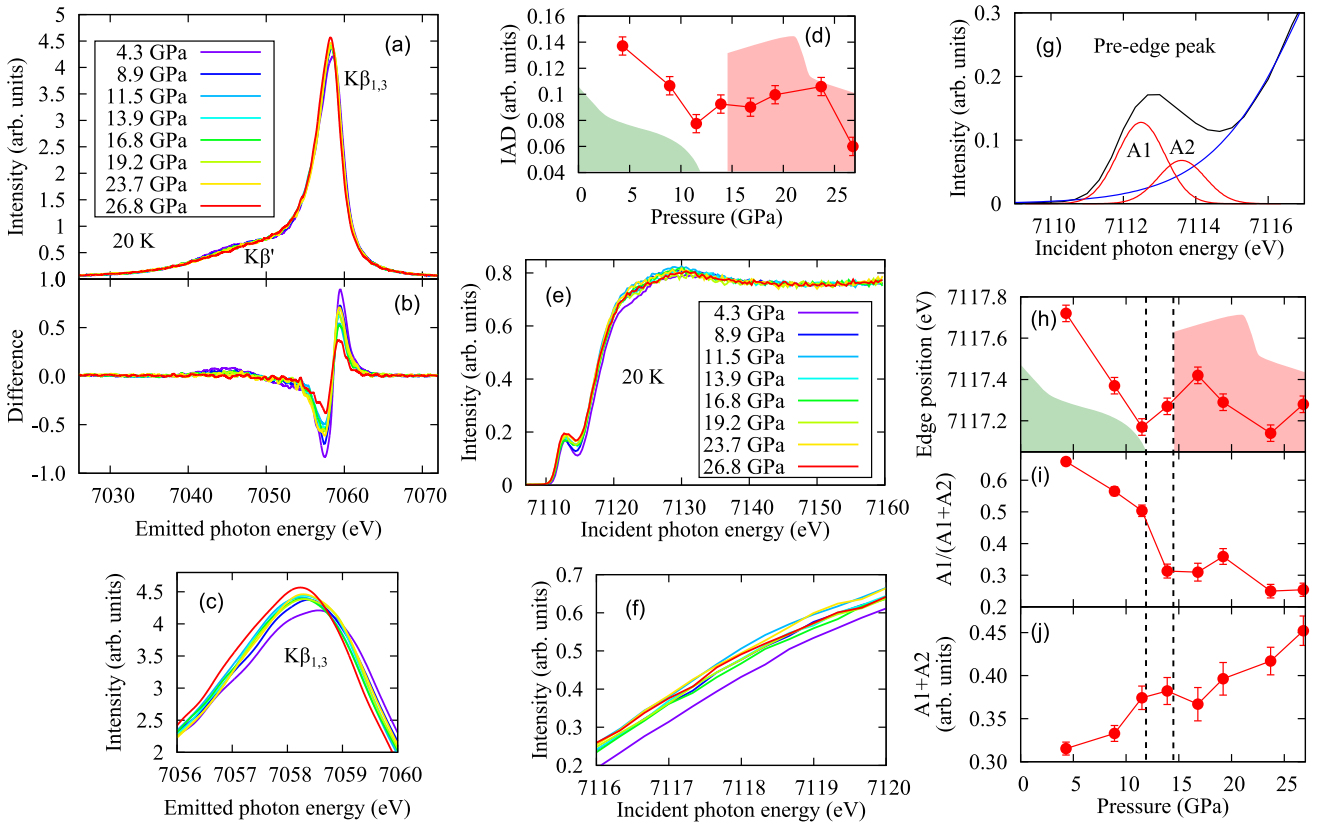

Fig. 2. (Color online) (a) Pressure dependence of $K\beta$ spectrum at 20 K. (b) Differences between the spectra between the spectra in (a) and that of FeCrAs, which is a non-magnetic reference sample with a local magnetic moment of $0\mu_B$. (c) Enlarged view of the $K\beta_{1,3}$ spectra around the peak in (a). (d) Pressure dependence of the IAD value. (e) Pressure dependence of the PFY-XAS spectrum at 20 K. (f) Enlarged view of the PFY-XAS spectra around the Fe-K absorption edge in (e). (g) Example of a fit to the pre-edge peak. (h–j) Pressure dependences of (h) energy of the absorption edge, (i) ratio of the A1 intensity to the total pre-edge peak intensity (A1+A2), and (j) total intensity of the pre-edge peak (A1+A2).

thus the electron–electron correlation. The pressure dependence of the magnetic moment strongly correlates to the change in electron–electron correlation under pressure and it decreases with pressure normally. Therefore, a possible increase of the electron–electron correlation found in the SC2 phase is highly anomalous.

Figure 2(e) shows the pressure dependence of the PFY-XAS spectrum at 20 K. The spectra are normalized by the areas in the energy range from 7140 to 7160 eV, which is far above the energy of the absorption edge. We also examined the normalization by the area of the whole energy range from 7105 to 7160 eV, but the difference of the results with these two normalization methods was little.[10] The intensity of the pre-edge peak and the energy of the absorption edge change with pressure. We fitted the pre-edge peak assuming two Gaussians (A1, A2) with an arctangent-like function as shown in Fig. 2(g). Figure 2(h) shows the pressure dependence of the energy of the absorption edge in the PFY-XAS spectra. The change in the edge energy corresponds to that in the Fe valence. The energy of the absorption edge (Fe valence), which is defined by half the value of the edge jump, decreases rapidly with increasing pressure in SC1. The edge energy rapidly recovers above 11.5 GPa then slowly decreases above 17 GPa in SC2. Figure 2(i) shows the pressure dependence of the ratio of the pre-edge peak areas, A1/(A1 + A2). This ratio corresponds to the unoccupancy rate of the e_g orbital because the A1 and A2 peaks are ascribed to the e_g and t_{2g} unoccupied orbitals, respectively.[23] The ratio decreases in SC1 and shows little change in SC2. Thus, the change in the Fe valence and the occupancy of the e_g orbital also show a clear difference between the two SC phases, and these changes appear to correlate with the T → cT transition. Figure 2(j) shows the total area of the pre-edge peak, A1+A2, which reflects the hybridization strength between Fe 3d and Se 4p electrons.[9,13] The result indicates that the hybridization increases monotonically with the pressure. This trend can be easily understood by considering the shrinkage of the lattice under pressure. Finally, we must comment on whether the significant changes of c/a [Fig. 1(d)] and edge position of PFY-XAS spectrum [Fig. 2(h)] show the phase where the SC2 appears. Firstly, such pressure-induced anomaly has not been observed in FeSe.[21] Secondly, any significant change of superconductivity has never been observed at ∼12 GPa in β-FeSe.[2] These results support that the changes observed at ∼12 GPa could cause the transition from SC1 to SC2 in $(NH_3)_yCs_{0.4}FeSe$. We also add that the superconducting volume fraction in the SC2 phase was maintained in a similar compound of $(NH_3)_yLi_x$-FeSe.[24]

To elucidate these experimental results in relation to the electronic and spin states, theoretical calculations of the spin Stoner factor, α^s, were performed for Cs_xFeSe model by introducing the rigid-band shift to the $Cs_{0.5}FeSe$ models based on the first-principles calculation with using the measured lattice constants at 8 K. Since the electronic structure is dominated by the FeSe layer, the Cs chemical

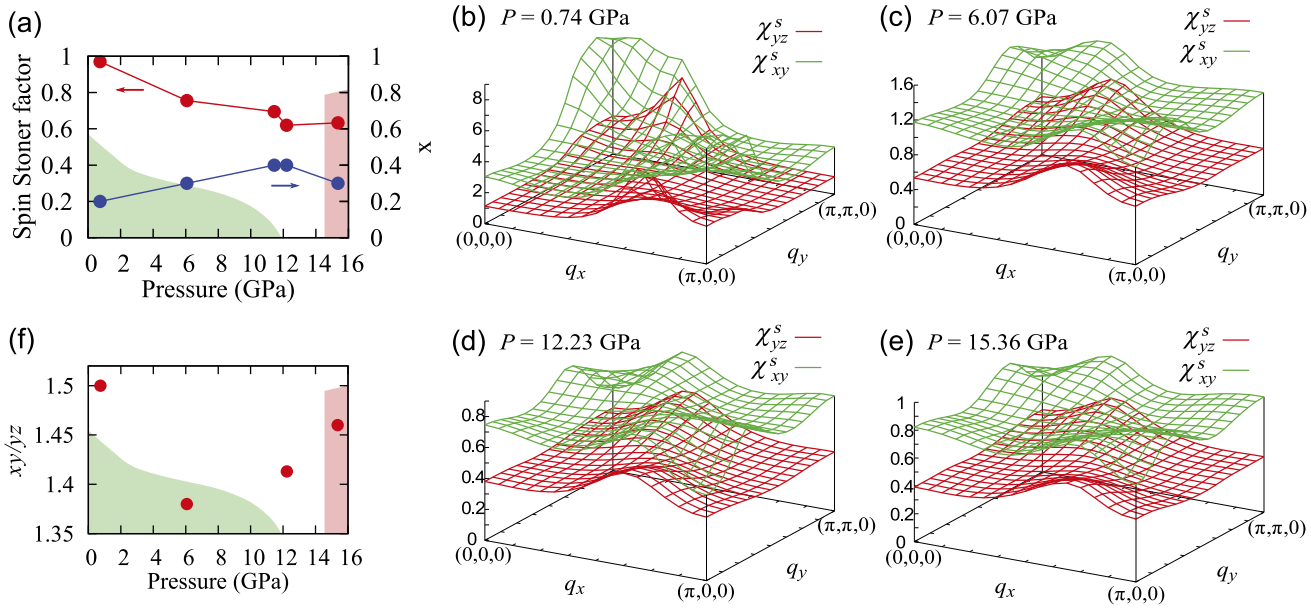

Fig. 3. (Color online) (a) Pressure dependence of calculated spin Stoner factor (red closed circles)[14] and assumed Cs chemical composition (blue closed circles) for Cs_xFeSe. (b–e) Calculated spin susceptibility χ^s at (b) $x = 0.2$ and $P = 0.74$ GPa, (c) $x = 0.3$ and $P = 6.07$ GPa, (d) $x = 0.4$ and $P = 12.23$ GPa, and (e) $x = 0.3$ and $P = 15.36$ GPa as functions of q_x and q_y. (f) Pressure dependence of the ratio of the maximum χ^s for the xy orbital to that for the yz orbital.

composition (x) controls the doping level. The pressure dependence of the Cs chemical composition (x) is determined to reproduce the pressure-induced change in the Fe valence estimated by the XAS spectra at Fe-K absorption edge, where the shift of the absorption edge corresponds to the charge transfer from the Cs site to the Fe site. Note that the spin susceptibility χ^s for the itinerant electrons diverges at $\alpha^s = 1$, where a long-range magnetic order is stabilized. Figure 3(a) shows that α^s decreases rapidly with increasing pressure in SC1, while it increases slightly in SC2. The pressure-induced change in the calculated α^s corresponds well to that in the IAD values. This may be because the spin susceptibility for itinerant electrons is correlated with the local magnetic moment in the mean field approximation. Figures 3(b)–3(e) show the pressure dependence of the spin susceptibility $\chi^s_{xy(yz)}$ for the $xy(yz)$ orbital as functions of q_x and q_y. We confirmed that the q_z dependence of χ^s is very small. The spin susceptibility decreases with increasing pressure in SC1 owing to the worse nesting. From the analogy to conventional Fe-based superconductors, the superconducting mechanism in SC1 is considered to be the fluctuation of the C_2 nematic orbital ($x^2 - y^2$-type charge quadrupole) enhanced by the spin fluctuations.[14,25] As shown in Fig. 3(f), the ratio of the maximum χ^s for the xy orbital to that for the yz orbital increases above 6 GPa. The results indicate that the T → cT phase transition is induced by the fluctuation of the C_4 orbital ($3z^2 - r^2$-type charge quadrupole) enhanced by the χ^s of xy orbital.[14] It is likely that the C_4 orbital fluctuation is the origin of the SC2 phase in the case that the SC2 is caused by the T → cT transition of the $(NH_3)_yCs_{0.4}FeSe$ phase.

In the SC1 phase, the lattice constant, local magnetic moment, Fe valence, and unoccupancy rate of e_g decrease monotonically with increasing pressure. It is known that the interlayer spacing of FeSe layers is strongly correlated with T_c and the degree of two-dimensionality.[5,26] This feature was also observed in SC1, where the pressure decreased the interlayer spacing of FeSe and T_c as a consequence of the decreasing lattice constant along the c-axis. As the crystalline electric field (CEF) becomes strong with increasing pressure, the e_g state for electrons becomes more favorable than at ambient pressure, resulting in the decrease in A1/(A1 + A2) and the local magnetic moment. The pressure-induced decrease in the Fe valence can be understood as the transfer of electrons from the Cs layer to the FeSe layer due to the reduction of the distance between the Cs and FeSe layers.

At the boundary between the SC1 and SC2 phases, the cT transition occurs, and then the local magnetic moment, Fe valence, and the occupancy rate of the e_g state change drastically as shown in Figs. 2(d), 2(h), and 2(i). These changes in the lattice, electronic structure, and spin state suggest that Fermi surface reconstruction occurs. The collapse of both the a- and c-axes results in the reduction of the Fe–Se bond length with the T → cT transition. The increase in the Fe valence could also be caused by the electron transfer from Fe to Se due to the reduction of the Fe–Se bond length. Further research is necessary to fully understand these charge transfer issues.

In the SC2 phase, the local magnetic moment increases slightly with pressure. Normally, the local magnetic moment decreases with increasing pressure because the CEF increases and the hybridization reduces the localization. However, the local magnetic moment, which is correlated with the electron–electron correlation, increases with pressure at the SC2 phase. Theoretically, the magnitude of the spin or orbital fluctuation increases with increasing electron–electron correlation, and this fluctuation could play a key role in inducing high-T_c superconductivity.[14,25]

4. Conclusion

In conclusion, we have studied the crystal, electronic structure, and spin states of $(NH_3)_yCs_{0.4}FeSe$ under pressure at low temperatures. The pressure dependence of the lattice

constants clearly showed the T → cT phase transition in $(NH_3)_yCs_{0.4}FeSe$ phase at a low temperature. Our results show distinct differences in both the crystal and electronic structures between the two SC phases. The experimental results suggest that the increase in the electron–electron correlation accompanying the increase in the magnetic moment may relate the high T_c in the SC2 phase. The present model calculations using the multi-orbital Hubbard model qualitatively showed a possible correlation between the spin Stoner factor and the local magnetic moment (i.e., electron–electron correlation). The spin susceptibility decreases in SC1 and the spin susceptibility for the *xy* orbital increases in SC2 accompanying the T → cT phase transition.[14)] The results suggest that near the T → cT transition pressure the C_4 orbital fluctuation prominently develops, which probably drives the SC2 phase by increasing the electron–electron correlation.[25)]

Acknowledgments The experiments were performed at Taiwan beamlines BL12XU and BL12B2 at SPring-8 under SPring-8 Proposal Nos. 2015B4260 and 2016B4264 (corresponding to NSRRC Proposal No. 2015-3-018) and at BL10XU under SPring-8 Proposal No. 2016B1725. The work at SPring-8 was supported by Grants-in-Aid for Scientific Research from the Japan Society for the Promotion of Science, KAKENHI 15K05914. We thank Riho Tanaka, Seika Shonai, and Lu Zheng for their help in the experiments. J.F.L. acknowledges support from HPSTAR.

1) G. R. Stewart, Rev. Mod. Phys. **83**, 1589 (2011).
2) S. Medvedev, T. M. McQueen, I. A. Troyan, T. Palasyuk, M. I. Eremets, R. J. Cava, S. Naghavi, F. Casper, V. Ksenofontov, G. Wortmann, and C. Felser, Nat. Mater. **8**, 630 (2009).
3) J. P. Sun, K. Matsuura, G. Z. Ye, Y. Mizukami, M. Shimozawa, K. Matsubayashi, M. Yamashita, T. Watashige, S. Kasahara, Y. Matsuda, J.-Q. Yan, B. C. Sales, Y. Uwatoko, J.-G. Cheng, and T. Shibauchi, Nat. Commun. **7**, 12146 (2016).
4) L. Sun, X.-J. Chen, J. Guo, P. Gao, H. Wang, M. Fang, X. Chen, G. Chen, Q. Wu, C. Zhang, D. Gu, X. Dong, K. Yang, A. Li, X. Dai, H.-K. Mao, and Z. Zhao, Nature (London) **483**, 67 (2012).
5) M. Izumi, L. Zheng, Y. Sakai, H. Goto, M. Sakata, Y. Nakamoto, H. L. T. Nguyen, T. Kagayama, K. Shimizu, S. Araki, T. C. Kobayashi, T. Kambe, D. Gu, J. Guo, J. Liu, Y. Li, L. Sun, K. Prassides, and Y. Kubozono, Sci. Rep. **5**, 9477 (2015).
6) Z. Yu, L. Wang, L. Wang, H. Liu, J. Zhao, C. Li, S. Sinogeikin, W. Wu, J. Luo, N. Wang, K. Yang, Y. Zhao, and H.-K. Mao, Sci. Rep. **4**, 7172 (2014).
7) Y. Nakajima, R. Wang, T. Metz, X. Wang, L. Wang, H. Cynn, S. T. Weir, J. R. Jeffries, and J. Paglione, Phys. Rev. B **91**, 060508 (2015).
8) D. Guterding, S. Backes, H. O. Jeschke, and R. Valent, Phys. Rev. B **91**, 140503 (2015).
9) Y. Yamamoto, H. Yamaoka, M. Tanaka, H. Okazaki, T. Ozaki, Y. Takano, J.-F. Lin, H. Fujita, T. Kagayama, K. Shimizu, N. Hiraoka, H. Ishii, K.-D. Tsuei, and J. Mizuki, Sci. Rep. **6**, 30946 (2016).
10) (Supplemental Material) It includes details of the experiments and the theoretical calculation.
11) L. Zheng, M. Izumi, Y. Sakai, R. Eguchi, H. Goto, Y. Takabayashi, T. Kambe, T. Onji, S. Araki, T. C. Kobayashi, J. Kim, A. Fujiwara, and Y. Kubozono, Phys. Rev. B **88**, 094521 (2013).
12) L. Zheng, X. Miao, Y. Sakai, M. Izumi, H. Goto, S. Nishiyama, E. Uesugi, Y. Kasahara, Y. Iwasa, and Y. Kubozono, Sci. Rep. **5**, 12774 (2015).
13) H. Yamaoka, High Pressure Res. **36**, 262 (2016).
14) S. Onari, Y. Yamakawa, and H. Kontani, Phys. Rev. Lett. **112**, 187001 (2014).
15) S. Onari, Y. Yamakawa, and H. Kontani, Phys. Rev. Lett. **116**, 227001 (2016).
16) T. Miyake, K. Nakamura, R. Arita, and M. Imada, J. Phys. Soc. Jpn. **79**, 044705 (2010).
17) L. Zheng, X. Miao, Y. Sakai, H. Goto, E. Uesugi, R. Eguchi, S. Nishiyama, K. Sugimoto, A. Fujiwara, and Y. Kubozono, Phys. Rev. B **93**, 104508 (2016).
18) T. Terao, X. Yang, X. Miao, L. Zheng, H. Goto, T. Miyazaki, H. Yamaoka, H. Ishii, Y.-F. Liao, and Y. Kubozono, Phys. Rev. B **97**, 094505 (2018).
19) G. Vankó, T. Neisius, G. Molnár, F. Renz, S. Kárpáti, A. Shukla, and F. M. F. de Groot, J. Phys. Chem. B **110**, 11647 (2006).
20) H. Gretarsson, A. Lupascu, J. Kim, D. Casa, T. Gog, W. Wu, S. R. Julian, Z. J. Xu, J. S. Wen, G. D. Gu, R. H. Yuan, Z. G. Chen, N.-L. Wang, S. Khim, K. H. Kim, M. Ishikado, I. Jarrige, S. Shamoto, J.-H. Chu, I. R. Fisher, and Y.-J. Kim, Phys. Rev. B **84**, 100509 (2011).
21) J. M. Chen, S. C. Haw, J. M. Lee, T. L. Chou, S. A. Chen, K. T. Lu, Y. C. Liang, Y. C. Lee, N. Hiraoka, H. Ishii, K. D. Tsuei, E. Huang, and T. J. Yang, Phys. Rev. B **84**, 125117 (2011).
22) R. S. Kumar, Y. Zhang, Y. Xiao, J. Baker, A. Cornelius, S. Veeramalai, P. Chow, C. Chen, and Y. Zhao, Appl. Phys. Lett. **99**, 061913 (2011).
23) T. E. Westre, P. Kennepohl, J. G. DeWitt, B. Hedman, K. O. Hodgson, and E. I. Solomon, J. Am. Chem. Soc. **119**, 6297 (1997).
24) P. Shahi, J. P. Sun, S. H. Wang, Y. Y. Jiao, K. Y. Chen, S. S. Sun, H. C. Lei, Y. Uwatoko, B. S. Wang, and J.-G. Cheng, Phys. Rev. B **97**, 020508(R) (2018).
25) Y. Yamakawa, S. Onari, and H. Kontani, Phys. Rev. X **6**, 021032 (2016).
26) T. Hatakeda, T. Noji, K. Sato, T. Kawamata, M. Kato, and Y. Koike, J. Phys. Soc. Jpn. **85**, 103702 (2016).